46th AIAA Aerospace Sciences Meeting and Exhibit
7 - 10 January 2008, Reno, Nevada

AIAA 2008-1317

PIV Visualization of Dynamic Stall VAWT and Blade Load Determination

Carlos Simão Ferreira* Gerard van Bussel† Fulvio Scarano‡
Gijs van Kuik§
Delft University of Technology, Delft, 2629 HS, The Netherlands

The increasing awareness of the need for environmentally sustainable housing and cities has driven the promotion of wind energy conversion systems for the built environment. One of the results of the development of solutions for the built environment is the reappearance of Vertical Axis Wind Turbines (VAWTs). In the built environment, the VAWT presents several advantages over the more common Horizontal Axis Wind Turbines (HAWTs), namely: its low sound emission (consequence of its operation at lower tip speed ratios), better esthetics due to its three-dimensionality, its insensitivity to yaw wind direction and its increased power output in skewed flow (see Mertens et al[1] and Simão Ferreira et al[2]).

The phenomenon of dynamic stall is an inherent effect of the operation of a VAWT at low tip speed ratios (λ). The presence of dynamic stall has significant impact on both load and power.

The paper focuses on evaluating the feasibility of estimating loads on Vertical Axis Wind Turbine (VAWT) blades in dynamic stall by velocity data acquired with Particle Image Velocimetry (PIV). The work uses both numerical and experimental data. Simulated velocity data from a Detached Eddy Simulation (DES) at space and time refinement equivalent to that obtained with PIV is used to estimate the error associated with the method. The method is then applied to experimental data to verify the influence of the complexity of the flow and determination of space and time derivatives.

The acquired data over the entire rotation is used to calculate the blade forces from the velocity data and its derivatives (solving the momentum equation), following the methodology presented by Noca et al[3] and Scarano et al.[4] The integration of the forces from the velocity field should overcome the difficulties and limitations presented by pressure sensors for local section loads, but involves the referred difficulties in determining the correct time-derivatives.

Nomenclature

V	Control volume
c	airfoil/blade chord, m
C_{F_x}	force in x-direction coefficient
C_{F_y}	force in y-direction coefficient
C_N	normal force coefficient
C_T	tangential force coefficient
D	rotor diameter, m
F	aerodynamic force, N
H	rotor height (blade span), m
k	reduced frequency
p	static pressure, Pa
p_∞	static pressure at infinity, Pa

*PhD Researcher, Faculty of Aerospace Engineering, Kluyverweg 1, 2629 HS, Delft, The Netherlands.
†Associate Professor, Faculty of Aerospace Engineering, Kluyverweg 1, 2629 HS, Delft, The Netherlands.
‡Associate Professor, Faculty of Aerospace Engineering, Kluyverweg 1, 2629 HS, Delft, The Netherlands.
§Professor, Faculty of Aerospace Engineering, Kluyverweg 1, 2629 HS, Delft, The Netherlands.

k	reduced frequency
R	rotor radius, m
S	Outer contour of control volume
S_b	Inner contour of control volume
t	time
T	stress tensor, m^2/s^2
u	local velocity, m/s
U_∞	Unperturbed velocity, m/s
α	angle of attack
λ	tip speed ratio $\Omega_{Rot}.R/U_\infty$
θ	azimuth angle
ρ	fluid density kg/m^3
ω	perturbation frequency, rad/s
Ω	vorticity, s^{-1}
Ω_{Rot}	angular velocity of rotor, rad/s
μ	dynamic viscosity

I. Introduction

The development of wind turbine aerodynamics requires extensive wind tunnel experimental research, not only to identify and understand physical processes but also to validate numerical models and quantify performance. Wind tunnel research is usually limited by its cost and mainly by the inability to correctly simulate real conditions (Reynolds number, reduced frequency, tip speed ratio) due to wind tunnel size and power.

Another constraint is the limited access to the flow or the inability/complexity of measuring certain flow properties. Currently, most experimental results on rotors are usually confined to pressure measurements over the surface and wake measurements of velocity or wake location.

The latest years have seen an increase of the application of Particle Image Velocimetry (PIV) to rotor aerodynamics, mainly in the characterization of the flow field in the wake of the rotor.

The theoretical evaluation of the momentum equation to determine the body force from velocity field data has been thoroughly developed (see Noca[3]). Current research by the authors aims at applying the theory to the unsteady flow of a VAWT in dynamic stall, identifying and developing the procedure to implement the method to PIV measurements.

II. Methodology

The research methodology is divided in five main parts, of which this paper comprises the third and fourth. The first part consisted on the evaluation of the 2D flow field of a VAWT in dynamic stall a low tip speed ratios (large angles of attack), which was conducted in the work of Simão Ferreira et al.[5] The visualization and quantification of the flow field in terms of the development of the shed vorticity and wake was used for the validation of the second part of the research, the development of a 2D Navier-Stokes model of the VAWT in dynamic stall (see Simão Ferreira et al[6] and[7]).

Several turbulence models where tested for the *2D Navier-Stokes* simulation, with the most accurate results obtained with a *DES* (*Detached Eddy Simulation*). The simulation managed to replicate the vorticity shedding process and wake development, both in phase and in magnitude.

The third part of the research methodology aims at using the velocity data from the *2D Navier-Stokes* simulation to test the feasibility of estimating the loads on a VAWT airfoil in dynamic stall using only the velocity data, as it would result from PIV measurements. The results are compared with the force data obtained in the simulation and a sensitivity analysis to time and space grid refinement is performed.

The fourth part of the research involves the application of the procedure to real experimental velocity data. A second experiment on a two bladed H-Darrieus VAWT is performed, and the flow field around of the blades at one azimuthal position is used to underline the challenges of applying the method to real experimental data.

III. The 2D Navier-Stokes simulation

The geometry of the model is a 2D representation of the experimental setup of Simão Ferreira et al.[5] The model's wall boundary conditions consists of two walls spaced $1.25m$ apart, where a $0.4m$ diameter single-bladed Darrieus VAWT is placed. The rotor is represented by an $0.05m$ chord *NACA0015* airfoil and the $0.05m$ rotor axis. The rotor axis is placed over the symmetry position of the wind tunnel. The inlet and outlet boundary conditions are placed respectively $10D$ upwind and $14D$ downwind of the rotor, allowing a full development of the wake.

The model includes a 2D spatial grid, simulating the conditions at the middle cross-section of the experimental setup. The grid is composed of four non-conformal sub-grids, each a structured grid of quadrilateral elements. Figure III presents a diagram of the shape and location of each sub-grid and the wall boundary conditions representing the airfoil/blade, wind tunnel walls and rotor axis (the flow inlet and outlet boundary conditions are not represented).

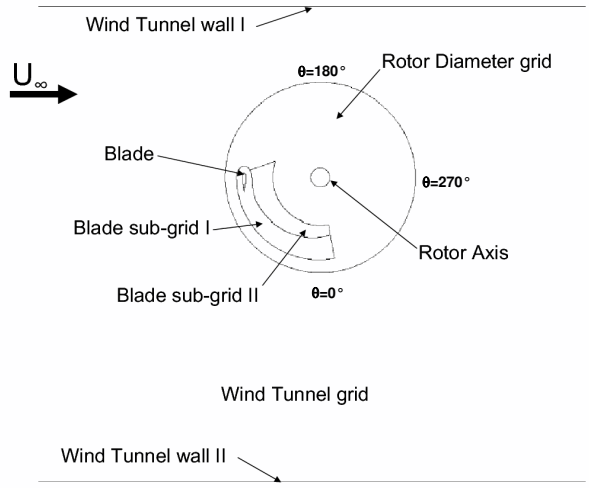

Figure 1. Diagram of the model geometry, sub-grid distribution and boundary conditions.

The use of moving sub-grids is necessary due to the movement of the rotor elements. Thus, the sub-grids *Rotor Diameter*, *Blade sub-grid I*, and *Blade sub-grid II* rotate with an angular velocity $\omega = 75rad/s$, while the sub-grid *Wind Tunnel* remains fixed. The grid comprises 3305 nodes over the airfoil surface, where the height of the first row of cells is set at a distance to the wall of $0.02\%c$ to ($y^+ \approx 1$ when $\theta = 90°$, $k-\epsilon$ model). The total model size comprises approx. $1.6 * 10^6$ cells.

A. Simulated flow conditions

The simulation aimed at representing the flow conditions of the experimental work for $\lambda = 2$ and incoming flow $U_\infty = 7.5m/s$. The level of unsteadiness is determined by the reduced frequency k, defined as $k = \omega \cdot c/2V$, where ω is the angular frequency of the unsteadiness, c is the blade's chord and V is the velocity of the blade. In this experiment, due to the variation of V with rotation angle, k was defined as $k = \omega \cdot c/(2\lambda \cdot V_\infty) = \omega \cdot c/(2\omega \cdot R) = c/(2R)$, where λ is the tip speed ratio and R is the radius of rotation. For this experimental work $k = 0.125$, placing the work in the unsteady aerodynamics region.

Due to the importance of the induction of the rotor, it is necessary to perform a simulation for several rotations until a fully developed wake is present. All values presented in this paper relate to the revolutions of the rotor after a periodic post-transient solution is found.

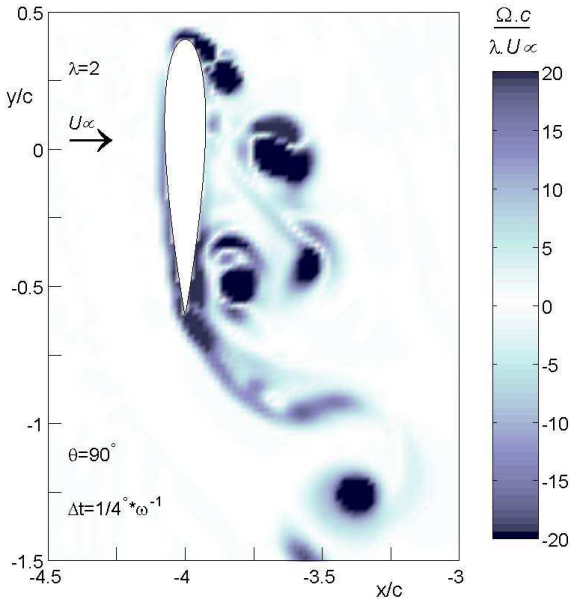

Figure 2. Vorticity field at $\theta = 90°$, *Detached Eddy Simulation.*

IV. Theoretical background

Consider a time-dependent control volume applied in a viscous unsteady flow, comprising a volume V [a] that is bounded by two surfaces S and S_B, as depicted in Figure 3. The fluid dynamic force per unit density F/ρ acting on the body can be expressed by Equation 1.

$$\begin{aligned} \frac{F}{\rho} = \quad & -\frac{d}{dt}\int_{V_{(t)}} \mathrm{u}\, dV \\ & + \oint_{S_{(t)}} \hat{\mathrm{n}} \cdot \left[-\frac{p}{\rho}\mathrm{I} - (\mathrm{u}-\mathrm{u_S})\,\mathrm{u} + \mathrm{T}\right] dS \\ & - \oint_{S_{b(t)}} \hat{\mathrm{n}} \cdot [(\mathrm{u}-\mathrm{u_S})\,\mathrm{u}]\, dS \end{aligned} \tag{1}$$

where T is the viscous stress tensor

$$T = \mu\left(\nabla \mathrm{u} + \nabla \mathrm{u}^{\mathrm{T}}\right) \tag{2}$$

The determination of fluid forces by the application of Equation 1 with PIV and other experimental data presents two main challenges:

1. the equation requires the determination of the velocity in the entire control volume; this is mostly unfeasible due to the difficulty of measuring in the boundary layer regions;
2. the equation requires the determination of the pressure over the outside contour of the control volume;

Noca et al[3] proposes a different formulation o the momentum balance: *the Flux Equation* (Equation 3)

$$\begin{aligned} \frac{F}{\rho} = \quad & + \oint_{S_{(t)}} \hat{\mathrm{n}} \cdot \gamma_{\mathrm{flux}}\, dS \\ & - \oint_{S_{b(t)}} \hat{\mathrm{n}} \cdot [(\mathrm{u}-\mathrm{u_S})\,\mathrm{u}]\, dS - \frac{d}{dt}\oint_{S_{b(t)}} \hat{\mathrm{n}} \cdot (\mathrm{ux})\, dS \end{aligned} \tag{3}$$

with the *flux term* γ_{flux}

[a] The notation presented by Noca et al[3] will be used for most of this work.

$$\begin{aligned}\gamma_{\text{flux}} = \quad & \tfrac{1}{2}\mathrm{u}^2\mathrm{I} - \mathrm{uu} - \tfrac{1}{N-1}\mathrm{u}\left(\mathrm{x}\times\omega\right) + \tfrac{1}{N-1}\omega\left(\mathrm{x}\times\mathrm{u}\right) \\ & -\tfrac{1}{N-1}\left[\left(\mathrm{x}\cdot\tfrac{\partial \mathrm{u}}{\partial t}\right)\mathrm{I} - \mathrm{x}\tfrac{\partial \mathrm{u}}{\partial t} + \left(N-1\right)\tfrac{\partial \mathrm{u}}{\partial t}\mathrm{x}\right] \\ & +\tfrac{1}{N-1}\left[\mathrm{x}\cdot\left(\nabla\cdot\mathrm{T}\right)\mathrm{I} - \mathrm{x}\left(\nabla\cdot\mathrm{T}\right)\right] + \mathrm{T}\end{aligned} \tag{4}$$

The flux equation require only terms of velocity and its derivatives over the boundaries of the control volume. For a 2D body with a solid wall S_b, this problems simplifies to determining the velocities and its time derivatives in the region of the outside contour S.

Yet, the elimination of the pressure term implies the appearance of the explicit formulation of the vorticity term ω. For the case of large wakes (bluff body flows) and good description of the velocity field on the wake, the *Flux Equation* is an efficient method to determine the loads on the body. For thin boundary layer, the relative coarseness of the measurement data can be a source of error. The asymptotic variation of vorticity over the contour as it crosses the wake can result in a significant numerical integration error; also, the averaging of the flow field due to the size of the interrogation window in the PIV processing can lead to an experimental measurement error/bias. This difficulty can be overcome by a change of reference frame where the origin is set at the wake, thus reducing the influence of the vorticity term at the wake.

A robust formulation to overcome the insufficient refinement of data at the wake is to explicitly express the pressure term (Equation 5).

$$\gamma_{\text{flux}} = \tfrac{\mathrm{p}}{\rho}\mathrm{I} - \mathrm{uu} - \tfrac{\partial \mathrm{u}}{\partial t}\mathrm{x} + \mathrm{T} \tag{5}$$

The disadvantage of this method is that it requires the estimation of the gradient of the pressure along the contour, once again coming across the problem of integration of a velocity gradient across the wake (Equation 6).

$$-\nabla\tfrac{\mathrm{p}}{\rho} = -\tfrac{\partial \mathrm{u}}{\partial t} + \left(\mathrm{u}\cdot\nabla\right)\mathrm{u} - \nabla\cdot\mathrm{T} \tag{6}$$

The error of estimation of the pressure gradient across the wake can be considered of little importance if the closed path of the pressure integration is set such that it starts and ends in the vicinity of the wake.

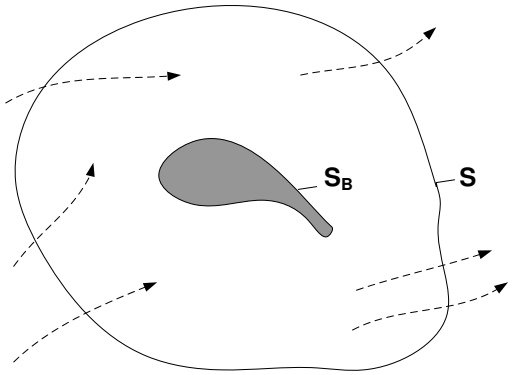

Figure 3. Representation of the control volume bounded by the outer contour S and the body contour S_B

V. Validation of the calculation of the pressure gradient

The accuracy of the estimation of the pressure can be evaluated in Figure 4; the figure presents the value of pressure (made non-dimensional) calculated by the 2D Navier-Stokes simulation and the pressure estimated by integration of the velocity field obtained from the simulation.

As seen in Figure 4, the effect of the error on the estimation of the pressure gradient at the location where the contour crosses the wake is local; notice that the pressure estimated from the velocity data is not

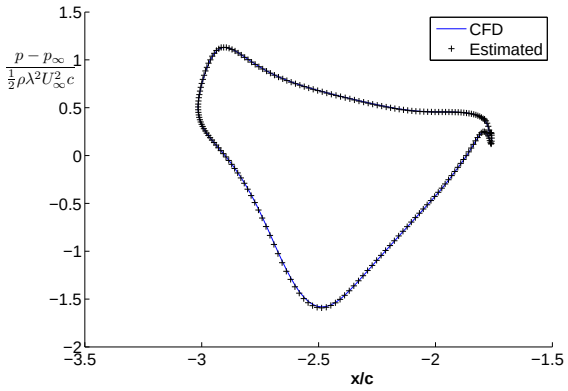

Figure 4. Pressure result from CFD simulation and estimated (integration of the velocity data) over contour *B*(Figure 5).

the actual pressure, but a value at a difference of a reference constant. For calculation of the force term, only the variation of the pressure is relevant. The absolute value of pressure can be estimated by integration of the gradient from the far-field.

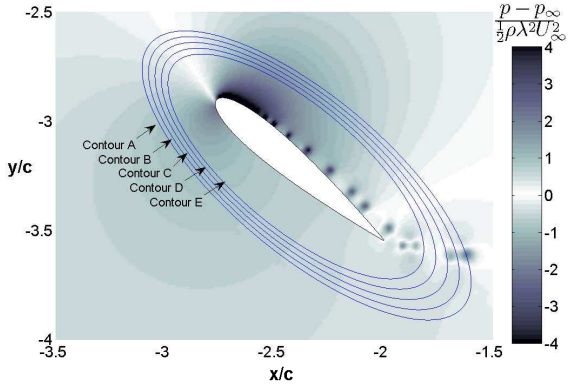

Figure 5. Location of volume contours *A*,*B*,*C* and *D*. Results of the integration of the forces around these contours are presented in Table 1.

VI. Comparison of the different formulations of the Flux Equation

In Table 1 the values of estimated *Normal Force Coefficient* $C_{N_{est}}$ and *Tangential Force Coefficient* $C_{T_{est}}$ are presented for different control volumes, defined by five different outer contours as presented in Figure 5. The results allow for two conclusions:

- the formulation with the explicit *Pressure* term (Equation 5) is less sensitive to the location of the contour than the conventional *Flux* formulation, especially the across the wake,
- the results for the *Pressure* formulation stand at an maximum difference of 5% for C_N and 10% for C_T to the 2D Navier-Stokes (CFD) calculated value.

The results show also that the result is largely insensitive to the choice of contour; this is under the condition that the contours avoid regions of large gradients.

	C_T		C_N	
	Flux	Pressure	Flux	Pressure
Contour A	-0.31	-0.28	2.62	2.65
Contour B	-0.27	-0.28	2.63	2.63
Contour C	-0.25	-0.26	2.65	2.65
Contour D	-0.27	-0.28	2.63	2.62
Contour E	-0.28	-0.29	2.62	2.61
CFD	-0.29		2.72	

Table 1. Comparison of C_N and C_T calculated by the *Flux* and *Pressure* method over different contours (see Figure 5). *CFD* value is obtained directly from the CFD simulation from airfoil surface integration.

VII. Sensitivity to spatial grid resolution

One of the limitations for the accurate integration of the forces is the resolution of the velocity grid. Figure 6 presents the values estimated (*Pressure* formulation) for C_N and C_T for different resolutions of the space grid. The grid is a regular uniform grid, where the scale of the grid represents $\Delta x/c = \Delta y/c$. The estimates prove to be significantly robust even at very coarse grids.

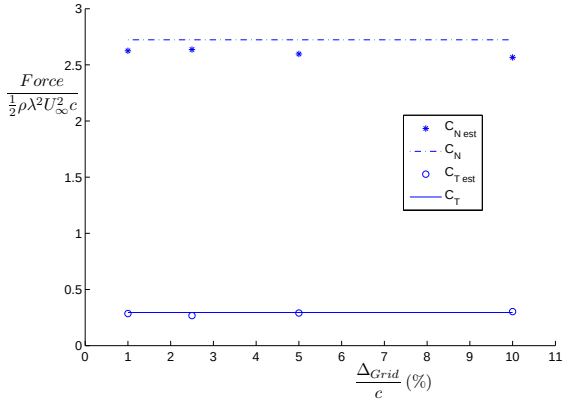

Figure 6. Effect of the resolution of the velocity field Δ_{Grid}/c).Comparison of CFD results for normal and tangential force coefficient C_N and C_T and the estimates from integration of the velocity field C_{Nest} and C_{Test}.

VIII. Sensitivity to phase/time grid resolution

The high reduced frequency of the flow ($k = 0.125$) implies that the time dependent terms play an important role in the force estimation. The velocity time derivative terms are estimated by Equation 7

$$\frac{\partial \mathrm{u}}{\partial t} = \frac{\mathrm{u}_\theta - \mathrm{u}_{\theta+\Delta\theta}}{\Delta\theta/\omega} \tag{7}$$

Figure 7 shows the variation of force coefficients for different time refinements for calculation of the time derivatives. The method shows little sensitivity to the error associated with the linear estimation of the time dependent terms.

IX. Comparison along rotation

Figure 8 presents the evaluation of the forces estimated versus those given by the CFD model. The method is effective even at large azimuthal angles, in highly complex flow, under the presumption that the time dependent terms are correctly estimated.

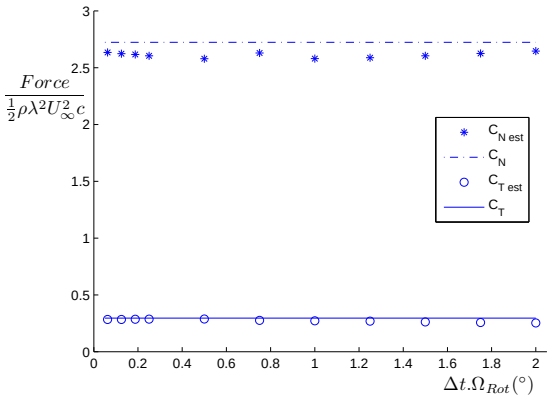

Figure 7. Effect of the size of time/phase step Δt for estimation of the velocity time derivatives. Comparison of CFD results for normal and tangential force coefficient C_N and C_T and the estimates from integration of the velocity field C_{Nest} and C_{Test} for different sizes of Δt.

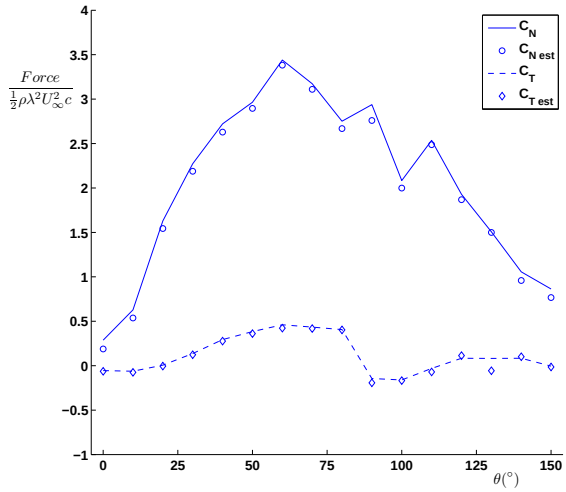

Figure 8. Comparison of CFD results for normal and tangential force coefficient C_N and C_T and the estimates from integration of the velocity field C_{Nest} and C_{Test} for $\theta = 0$ to 150.

X. Application to experimental data

The estimation of loads on a VAWT airfoil undergoing dynamic stall by integration of the velocity data is proven feasible in the previous sections, by using velocity data from a 2D Navier-Stokes simulation. Yet, application to real data adds the uncertainty resulting from experimental error and the estimation of the time and spatial derivatives of the velocity.

To investigate the difficulties of implementation of the method to a real VAWT in a wind tunnel, an second experimental component was added to the current research.

In this experiment, the flow field around the mid section of a two bladed H-Darrieus was measured in a Stereo PIV configuration. For the purpose of this paper, only a 2D analysis of the data is performed.

XI. Experimental setup

A. The Wind Tunnel

The experimental work was performed in the Low-Speed Low-Turbulence Wind Tunnel of the Faculty of Aerospace Engineering of Delft University of Technology (TU Delft). This tunnel has a contraction ratio of 17.6, giving a maximum test section velocity of 100 m/s and a low turbulence intensity ranging from .015% at $10m/s$ to .07% at $75m/s$. The octagonal test section is 1.80 m wide, 1.25 m high and 2.60 meters long.

B. The Model

The model is a two bladed H-Darrieus Vertical Axis Wind Turbine. The rotor diameter is $D = 0.57m$ with a height $H = 0.50m$. The blades have a *NACA0015* and *NACA0018* profiles, with chord $c = 0.06m$, and elliptic tips.

The blades are supported on the axis by two spars at $0.15m$ from each side of the blade mid section and two tension wires at $0.05m$. The model was placed in the center of the test section, with the axis of rotation at mid-height. The results presented in this paper focus on the passage upwind of the midsection with *NACA0015* profile at the $\theta = 20°$ position (Figure 9).

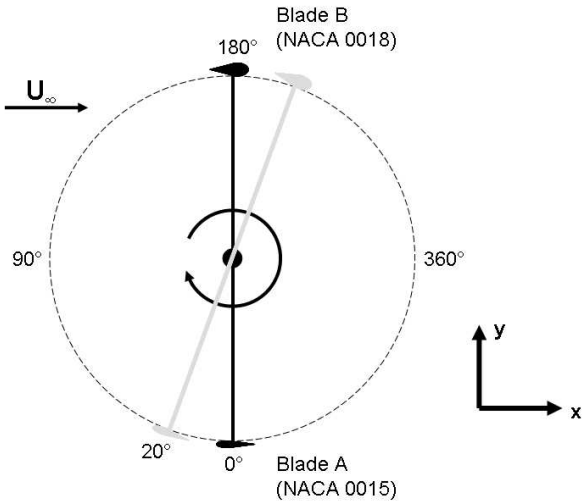

Figure 9. Schematic of experiment. Results focus on *Blade A* (NACA0015) at the $\theta = 20°$ position (light grey representation).

C. PIV system and setup

The PIV system used consists of a double-cavity Nd:YAG laser (400 mJ/ pulse) combined with a acquisition and control unit. A light sheet is introduced vertically from the test section, perpendicular to the blade and

located at its mid span. The flow was seeded with $1.5\mu m$ droplets generated by a fog machine. Two CCD camera at $1200 * 1240$ pixels setup. The interval was set at $40\mu s$.

XII. Data acquisition

The total flow field around the airfoil was built from two separate measurements. Between the two measurements the laser and cameras were replaced too acquire data in the shadow region of the previous measurement setup. This requirement of the setup creates an uncertainty on the relative correct location of the two halves of the assembled field of view. A total of 60 samples per azimuthal position were acquired. Phase difference between sets of samples was set at intervals of $\Delta\theta = 0.3°$ and $\Delta\theta = 2.0°$.

XIII. Phase averaging

The analysis of the flow and dynamic stall development assumes the existence of a dominant phase locked average flow field, determined by the azimuthal position of the blade. The instantaneous flow is the result of this phase locked average flow field plus a random one.

The standard method of obtaining the average unsteady flow field consists of averaging (with or without a weighing filter) the several instantaneous velocity fields. Figure 10 presents the phase locked average velocity field around the blade.

The source of this high variability of a single point velocity value is the result of the complex vortical structures released over the airfoil's sides (which present randomness both in strength and in location) and its development in the wake.

For a tip speed ratio of $\lambda = 4$, at $\theta = 20°$ a phenomenon of Blade-Vortex-Interaction occurs. The blade crosses two wakes: the wake generated by the second blade and the wake generated by the blade itself in the previous rotation (see Figure 11).

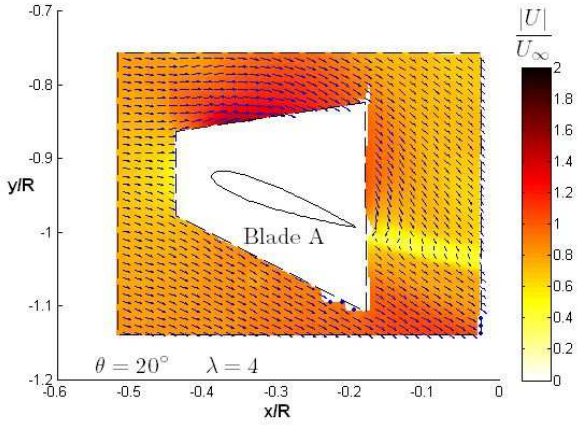

Figure 10. Velocity around *Blade A* (*NACA0015* profile) at $\theta = 20°$.

XIV. Flow acceleration term

The time dependent terms are estimated from the difference in phase of two phase phase locked velocity averages. The phase difference used is $\Delta\theta = 2.0°$; this value is sufficiently large such that the phase difference in the velocity field is significantly larger than the random oscillations between samples. Figure 12 show the flow acceleration term estimated from the difference between the two average flow fields.

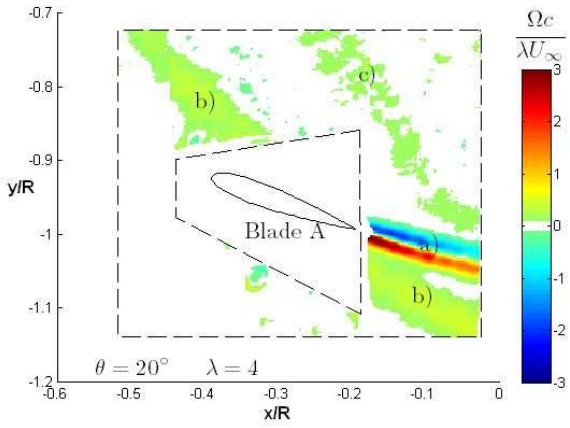

Figure 11. Vorticity around *Blade A* (*NACA0015* profile) at $\theta = 20°$. The image shows three different wake segments: a) the wake shed by *Blade A*; b) the wake shed by *Blade B*; and c) the wake shed by *Blade A* in the previous revolution.

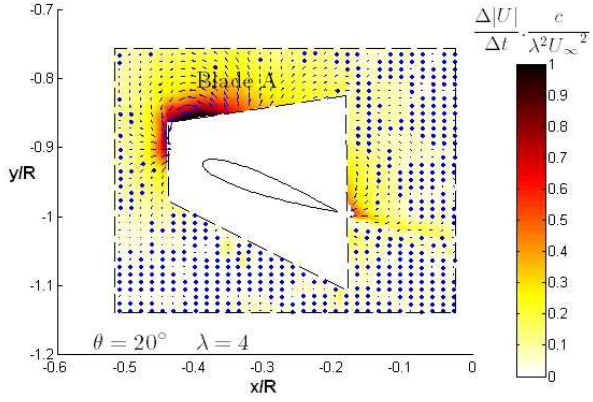

Figure 12. $\partial|V|/\partial t$ term (approximated by $\Delta|V|/\Delta t$) around *Blade A* (*NACA0015* profile) at $\theta = 20°$.

XV. Analysis of the determination of blade loads

Two of the large sources of error in the experimental data is the determination of the time derivatives and spatial derivatives of the velocity, specially across the wakes of in the regions of strong gradients as close to the airfoil. To exemplify the associated error, we will estimate the force coefficients in x and y direction on sections of the flow without any body inside. From theory, these forces should be zero, and any difference form zero result from error on the estimation of the real velocity or its derivatives. Figure 13 shows the location of three contours in the flow field. Table 2 shows the value of the force coefficients for these three contours. The results show that a small error occurs even in areas of flow with low amount of vorticity or acceleration.

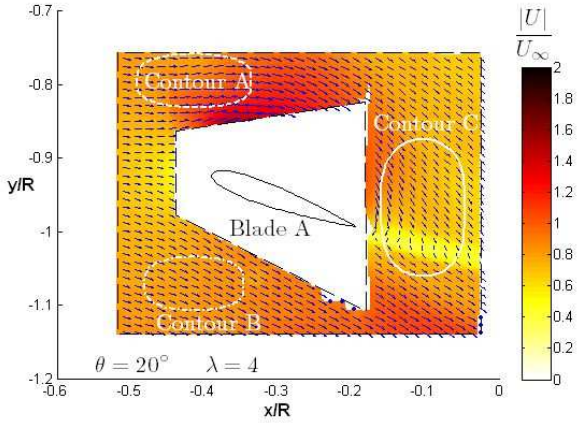

Figure 13. Contours *A*, *B* and *C* on velocity field near *Blade A* (*NACA0015* profile) at $\theta = 20°$.

	C_{F_x}	C_{F_y}
Contour A	0.0119	-0.0198
Contour B	-0.0068	0.0026
Contour C	0.0019	0.0101

Table 2. Comparison of C_{F_x} and C_{F_y} calculated for three different contours (see Figure 13). not surrounding the blade.

Applying now the estimation to the forces around the airfoil at three different contours 14, it is possible to estimate the coefficients for tangential and normal force (Table 3). The results present differences ±10%.

	C_T	C_N
Contour A	0.115	0.736
Contour B	0.120	0.778
Contour C	0.131	0.678

Table 3. Comparison of C_T and C_N calculated for three different contours (see Figure 14) surrounding the blade.

XVI. Conclusions

The estimation of loads on a VAWT airfoil undergoing dynamic stall by integration of the velocity data is proven feasible. The sensitivity analysis with *CFD* data have shown that the method is robust to contour location, velocity data grid refinement and linear estimation of the velocity time derivative. The *Flux*

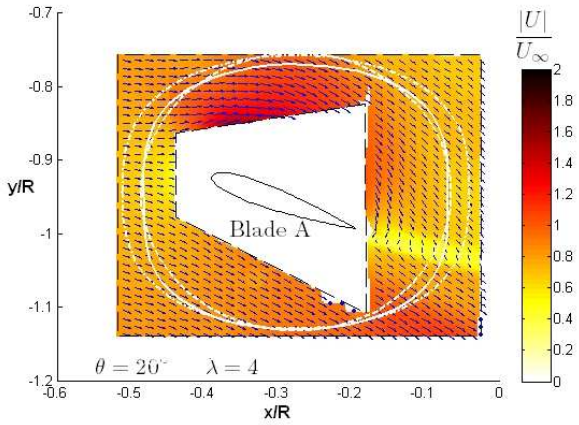

Figure 14. Contours *A*, *B* and *C* on velocity field around *Blade A* (*NACA0015* profile) at $\theta = 20°$.

Equation formulation from Noca et al[3] proved effective, as it did an explicit integration of the pressure term over the outer contour of the control volume. The integration across the wake requires a change of reference frame to overcome the influence of the error on estimating the strong velocity gradient. The method was validated over the development of dynamic stall from $\theta = 0°$ to $\theta = 150°$.

Application to experimental data also shows the feasibility of the method, even in highly complex flows. Yet, the results show that, due to the complexity of the flow, future research will focus on the development of setup and estimation procedures to overcome the uncertainty associated with the estimation of the time and spatial derivatives.

References

[1]Mertens, S., van Kuik, G., and van Bussel, G., "Performance of a H-Darrieus in the Skewed Flow on a Roof," *Journal of Solar Energy Engineering*, Vol. 125, 2003, pp. 433–440.

[2]Simão Ferreira, C., van Bussel, G., and van Kuik, G., "Wind tunnel hotwire measurements, flow visualization and thrust measurement of a VAWT in skew," *AIAA/ASME Wind Energy Symposium*, 2006.

[3]Noca, F., Shiels, D., and Jeon, D., "A comparison of methods for evaluating time-dependent fluid dynamic forces on bodies, using only velocity fields and their derivatives," *Journal of Fluids and Structures*, Vol. 13, 1999, pp. 551–578.

[4]van Oudheusden, B., Scarano, F., Roosenboom, E., E.W.F.Casimiri, and L.J.Souverein, "Evaluation of integral forces and pressure fields from planar velocimetry data for incompressible and compressible flows," *Experiments in Fluids*, 2007.

[5]Simão Ferreira, C., van Bussel, G., van Kuik, G., and Scarano, F., "2D PIV visualization of dynamic stall on a vertical axis wind turbine," 45^{th} *AIAA Aerospace Sciences Meeting and Exhibit /ASME Wind Energy Symposium*, 2007.

[6]Simão Ferreira, C., van Bussel, G., and van Kuik, G., "2D CFD simulation of dynamic stall on a vertical axis wind turbine: verification and validation with PIV measurements," *Abstract submited for the 2007 AIAA/ASME Wind Energy Symposium*, 2007.

[7]Simão Ferreira, C., van Bussel, G., van Kuik, G., and Bijl, H., "Simulating dynamic stall in a 2D VAWT: verification and validation with Particle Image Velocimetry data," *The Science of Making Torque from Wind*, 2007.